

Original article

Imbibition behaviors in shale nanoporous media from pore-scale perspectives

Han Wang¹, Jianchao Cai¹^{*}, Yuliang Su^{2,3}, Zhehui Jin⁴^{*}, Wendong Wang^{2,3}, Guanqun Li⁵

¹National Key Laboratory of Petroleum Resources and Engineering, China University of Petroleum, Beijing 102249, P. R. China

²Key Laboratory of Unconventional Oil & Gas Development (China University of Petroleum (East China)), Ministry of Education, Qingdao 266580, P. R. China

³School of Petroleum Engineering, China University of Petroleum (East China), Qingdao 266580, P. R. China

⁴School of Mining and Petroleum Engineering, Department of Civil and Environmental Engineering, University of Alberta, Edmonton, AB T6G 1H9, Canada

⁵Exploration and Development Research Institute, Shengli Oilfield Company, Sinopec, Shandong 257015, P. R. China

Keywords:

Spontaneous imbibition
fluid-fluid interfacial slip
intermolecular interactions
lattice Boltzmann method
nanoporous media
water saturation

Cited as:

Wang, H., Cai, J., Su, Y., Jin, Z., Wang, W., Li, G. Imbibition behaviors in shale nanoporous media from pore-scale perspectives. *Capillarity*, 2023, 9(2): 32-44.

<https://doi.org/10.46690/capi.2023.11.02>

Abstract:

In shale reservoirs, spontaneous imbibition is an important mechanism of fracturing fluid loss, which has an important impact on enhanced oil recovery and water resource demand. However, spontaneous imbibition behaviors are more complicated to characterize and clarify due to the nanoscale effects of the boundary slip, oil-water interfacial slip, and heterogeneous fluid properties caused by intermolecular interactions. A nanoscale multi-relaxation-time multicomponent and multiphase lattice Boltzmann method was applied to investigate the water imbibition into oil-saturated nanoscale space. The effects of pore size, fluid-surface slip, water film, oil-water interfacial slip, water bridge, and pore structures on the imbibition behaviors in a single nanopore were investigated. Then, the spontaneous imbibition behaviors in nanoporous media based on the pore scale microsimulation parameters obtained from the molecular simulation velocity results were simulated, and the effects of water saturations on imbibition behaviors were discussed. The results show that as the water saturation increases from 0 to 0.1, the imbibition mass in nanoporous media increases because of the oil-water interfacial slip and a completely hydrophilic wall. As water saturation continues to increase, the imbibition mass decreases gradually because the existence of water bridges impedes the water imbibition.

1. Introduction

Spontaneous imbibition in porous media has received much attention for its importance in many fields, such as, ink-jet printing, soil infiltration, rainwater infiltration building and oil/gas engineering (Abd et al., 2019; Hodder and Nychka, 2019; Siddiqui et al., 2019; Cai et al., 2021). For unconventional oil/gas resources, shale/tight oil/gas production predominantly relies on horizontal drilling and hydraulic fracturing (Siddhamshetty et al., 2019; Deng et al., 2022), resulting in fracturing fluids entering pore spaces through spontaneous

imbibition (Akbarabadi et al., 2017; Li et al., 2019; Siddiqui et al., 2019; Tu and Sheng, 2020; Wijaya and Sheng, 2021; Xu et al., 2021). Spontaneous imbibition can incur fracturing fluid loss, which is important to the efficacy of enhanced oil recovery (Singh, 2016; Al-Ameri et al., 2018; Siddiqui et al., 2019). The pore size in shale reservoirs is generally 2-200 nm, and the oil/water molecular size is comparable to the pore size, which causes the nonnegligible strong intermolecular interactions (Saraji and Piri, 2015; Zhou et al., 2016; Yuan et al., 2017; Zhang et al., 2020b). Hence, due to nanoscale effects of the boundary slip, fluid-fluid interfacial slip and heteroge-

neous fluid properties caused by intermolecular interactions, the spontaneous imbibition behaviors are more complicated to characterize and clarify by the conventional imbibition theory (Zhang et al., 2017, 2018; Zeng et al., 2020). In addition, water may occupy pores during the formation and evolution of natural reservoirs (Guan et al., 2016; Li et al., 2016, 2017), resulting in complex capillary forces inevitably influencing spontaneous imbibition processes. Therefore, the effects of intermolecular interactions and primary water need to be taken into account for the spontaneous imbibition behaviors in nanoporous media.

Spontaneous imbibition can be attributed to the collective effect of viscous force (P_v), capillary force (P_c), inertial force (P_i), and the density difference resultant gravitational pressure gradient (P_g), according to their relationship $P_c - P_g = P_v + P_i$ (Tu and Sheng, 2020; Cai et al., 2021; Wang et al., 2021a). In shale nanopores, capillary force is particularly important, gravity becomes negligible (Sheng et al., 2017), and viscous force depends on oil/water-surface non-zero slip velocity (Wang et al., 2016) and heterogeneous fluid properties (Wu et al., 2019). A number of experimental studies focus on the effect of wettability alteration (from oil-wet to water-wet) and interfacial tension (IFT) reduction on capillary forces to improve shale oil recovery via spontaneous imbibition (Patil et al., 2018; Liu et al., 2019; Saputra et al., 2019; Shao et al., 2023). However, the core-based imbibition experiments cannot quantitatively nor qualitatively analyze the complex oil-water mechanisms in nanopores at the microscopic scale (Chen et al., 2023). Recently, Lu et al. (2022) reported an experimental study on oil capillary imbibition in nanochannels with the width ranging from 34 nm to 100 nm based on nanofluidic chips. They found that the imbibition process is much slower than that in the theoretical prediction. In 34 nm wide nanochannels, the actual imbibition process is 60% slower due to strong fluid-surface interactions, which significantly increase flow resistance (Lu et al., 2022). On the other hand, molecular dynamics (MD) simulations can model imbibition behaviors in nanopores by explicitly considering intermolecular interactions. Yang et al. (2017) studied octane and water imbibition into graphite and quartz slit pores by using MD simulations. They reported that oil uptake in graphite pores is significantly higher than water uptake. Sang et al. (2022) conducted MD simulations to study the imbibition of *n*-alkane into kerogen slit pores and investigated the effect of pore width, temperature, and *n*-alkane types on penetration speed, dynamic contact angle, and molecular conformations. Feng et al. (2018) adopted a molecular kinetics approach to explain the unexpected $t^{1/2}$ -dependence of capillary filling behaviors at the molecular level, and highlighted the importance of effective viscosity and true slip on imbibition in nanopores. However, most of these studies are limited to gas-liquid two-phase imbibition, while oil-water two-phase imbibition has been rarely studied. In addition, due to expensive computational cost, these MD studies mainly focus on single nanopore cases. On the other hand, a few studies established theoretical methods for imbibition behaviors based on the single nanopore and capillary bundle model (Wang et al., 2021a; Cai et al., 2022; Li et al., 2022; Weibing et al., 2022). Wang et al. (2021a) and Weibing et

al. (2022) studied the water imbibition into nanopores, and the molecular interactions, dynamics contact angle, entrance and inertia effects were considered. Although these methods have negligible computational cost, they cannot consider the complex oil-water distributions and porous media structures.

Pore-scale simulations have become an effective tool to simulate the imbibition behaviors under complex oil-water distributions and pore structures, which include the experiments on microfluidic chips (Mehmani et al., 2019; Tsao et al., 2021), computational fluid dynamic coupling Navier-Stokes equations (Zhu et al., 2019), pore network modeling (Wang and Sheng, 2018, 2020; Zhao et al., 2022), lattice Boltzmann method (LBM) (Wiklund and Uesaka, 2013; Zhao et al., 2021; Chen et al., 2022; Zhou et al., 2023), and dissipative particle dynamics method (Chen et al., 2012; Ruiz-Morales and Alvarez-Ramírez, 2021), etc. Among them, LBM is one of the most popular pore-scale simulation methods for multiphase flow in porous media thanks to its efficiency and efficacy in terms of handling complex pore structures (Liu et al., 2022). However, the current LBM simulations on imbibition mainly focus on the conventional scale, which are not suitable for nanoporous media. Although Zheng et al. (2018) proposed an improved pseudo-potential LBM to simulate spontaneous imbibition behaviors in a shale porous structure, the fluid-solid and fluid-fluid molecular interactions were not considered. In nanochannels, the strong intermolecular interaction forces can lead to nanoscale effects such as fluid-solid boundary slip, fluid-fluid interfacial slip and heterogeneous fluid properties (Mattia and Calabrò, 2012; Secchi et al., 2016; Kannam et al., 2017; Zhan et al., 2020a, 2020b; Weibing et al., 2022), which have a pronounced impact on the oil-water viscous force. Therefore, it is necessary to consider these nanoscale effects when LBM is used to study spontaneous imbibition behavior in nanoporous media.

In this study, a nanoscale LBM which can consider the fluid-surface boundary slip, fluid-fluid interfacial slip and heterogeneous fluid properties due to intermolecular interactions is used to simulate oil-water imbibition behaviors in nanoporous media. The effect of pore size, fluid-surface slip, oil-water interfacial slip, water film, water bridges and pore structures on single-pore imbibition behaviors are discussed. In addition, the physical parameters in the proposed model are adjusted by fitting MD results to simulate water imbibition into quartz nanoporous media. This study investigates natural imbibition behaviors in nanopores and nanoporous media, and quantitatively analyzes the effect of nanoscale effects under various water distributions and saturation.

2. Nanoscale multi-relaxation time LBM

In our previous studies, the fluid-surface slip, oil-water interfacial slip and heterogeneous fluid properties are incorporated into LBM to simulate oil-water two-phase flow in shale nanoporous media (Wang et al., 2022, 2023). In this work, this model is applied to study imbibition behaviors, and the physical properties of the oil and water can be found. For multi-relaxation time LBM, the evolution equation is given by (Lallemand and Luo, 2000):

$$\mathbf{f}^\sigma(\mathbf{x} + \mathbf{e}_\alpha \delta_t, t + \delta_t) - \mathbf{f}^\sigma(\mathbf{x}, t) = -\mathbf{M}^{-1} \Lambda \mathbf{M} (\mathbf{f}^\sigma(\mathbf{x}, t) - \mathbf{f}^{eq, \sigma}(\mathbf{x}, t)) + \delta_t \mathbf{F}^\sigma \quad (1)$$

where $\mathbf{f}^\sigma(\mathbf{x}, t)$ is the density distribution function of σ component at \mathbf{x} position and time t , $\alpha = 0, 1, 2, \dots, 8$ are the nine directions of D2Q9 model, \mathbf{e}_α is the velocity at α direction, δ_t is the time step, Λ is the relaxation diagonal matrix, $\mathbf{f}^{eq, \sigma}$ is the equilibrium density distribution function, \mathbf{F}^σ is the external force, \mathbf{M} is the transformation matrix.

With the transformation matrix \mathbf{M} , Eq. (1) can be rewritten as:

$$\mathbf{m}'^\sigma = \mathbf{m}^\sigma - \Lambda (\mathbf{m}^\sigma - \mathbf{m}^{eq, \sigma}) + \delta_t \left(\mathbf{I} - \frac{\Lambda}{2} \right) \mathbf{S}^\sigma \quad (2)$$

where $\mathbf{m}^\sigma = \mathbf{M} \mathbf{f}^\sigma$, $\mathbf{m}^{eq, \sigma} = \mathbf{M} \mathbf{f}^{eq, \sigma}$ are 9-dimensional vectors for the moments and the equilibria of moments, respectively, \mathbf{I} is the unit tensor, $\mathbf{S}^\sigma = \mathbf{M} \mathbf{S}'^\sigma$ is the forcing term in the moment space, the external force is defined by $\mathbf{F}^\sigma = \mathbf{M}^{-1} \left(\mathbf{I} - \frac{\Lambda}{2} \right) \mathbf{M} \mathbf{S}'^\sigma$. $\mathbf{F}^\sigma = \mathbf{F}_{int, \sigma} + \mathbf{F}_{ads, \sigma} + \mathbf{F}_{b, \sigma}$, and $\mathbf{F}_{int, \sigma}$ is the interaction force on the component σ , $\mathbf{F}_{ads, \sigma}$ is the interaction force between component σ and the solid wall, $\mathbf{F}_{b, \sigma}$ is the external body force. For multi-component multi-phase flow, they can be expressed as:

$$\begin{aligned} \mathbf{F}_{int, \sigma}(\mathbf{x}, t) &= -G_{\sigma\sigma'} \psi_\sigma(\mathbf{x}, t) \sum_{\alpha} w(|\mathbf{e}_\alpha|^2) \psi_{\sigma'}(\mathbf{x} + \mathbf{e}_\alpha \delta_t) \mathbf{e}_\alpha \\ &\quad - G_{\sigma\sigma} \psi_\sigma(\mathbf{x}, t) \sum_{\alpha} w(|\mathbf{e}_\alpha|^2) \psi_\sigma(\mathbf{x} + \mathbf{e}_\alpha \delta_t) \mathbf{e}_\alpha \end{aligned} \quad (3)$$

$$\mathbf{F}_{ads, \sigma}(\mathbf{x}, t) = -G_{\sigma s} \psi_\sigma(\mathbf{x}, t) \sum_{\alpha} w(|\mathbf{e}_\alpha|^2) s(\mathbf{x} + \mathbf{e}_\alpha \delta_t) \mathbf{e}_\alpha \quad (4)$$

$$\mathbf{F}_{b, \sigma} = (F_{\sigma, b, x}, F_{\sigma, b, y}) \quad (5)$$

where $G_{\sigma\sigma'}$ is a parameter controlling the liquid-liquid strength, σ' represent the other phase, $G_{\sigma s}$ is a parameter controlling the strength of the fluid-solid force, s is an indicator function equaling to 0 and 1 for fluid and solid nodes, ψ_σ is pseudopotential, $\psi_\sigma = 1 - \exp(-\rho_\sigma)$, $w(|\mathbf{e}_\alpha|^2)$ is the weight, $w(1) = 1/3$, $w(2) = 1/12$.

In order to accurately simulate spontaneous imbibition in nanochannels, the collective nanoscale effects of fluid-surface slip, oil-water interfacial slip and heterogeneous viscosity need to be explicitly considered. For fluid-surface slip, the modified combined boundary conditions of half-way bounce back and diffusive Maxwell's reflection (Wang et al., 2022) can be applied to achieve oil-water two-phase non-zero boundary velocity, which is regarded as boundary slip, which is given as:

$$\begin{aligned} f_{\sigma, \alpha} &= (1 - r_\sigma) \overline{f_{\sigma, \bar{\alpha}}} \\ &\quad + r_\sigma \frac{\sum_{\alpha} s(\mathbf{x} + \mathbf{e}_\alpha \delta_t) \overline{f_{\sigma, \bar{\alpha}}}}{\sum_{\alpha} s(\mathbf{x} + \mathbf{e}_\alpha \delta_t) f_{\sigma, \alpha}^{eq}(\mathbf{u}_{\sigma, wall})} f_{\sigma, \alpha}^{eq}(\mathbf{u}_{\sigma, wall}) \end{aligned} \quad (6)$$

where $\overline{f_{\sigma, \bar{\alpha}}}$ is the post-collision density distribution function in $\bar{\alpha}$ direction, in which $\bar{\alpha}$ is the inverse direction of α , $\mathbf{u}_{\sigma, wall}$ is the wall velocity, r_σ is a combination parameter to characterize the degree of boundary slip. As r_σ increases, fluid-surface slip velocity increases.

For oil-water interfacial slip, the viscosity of the oil-water

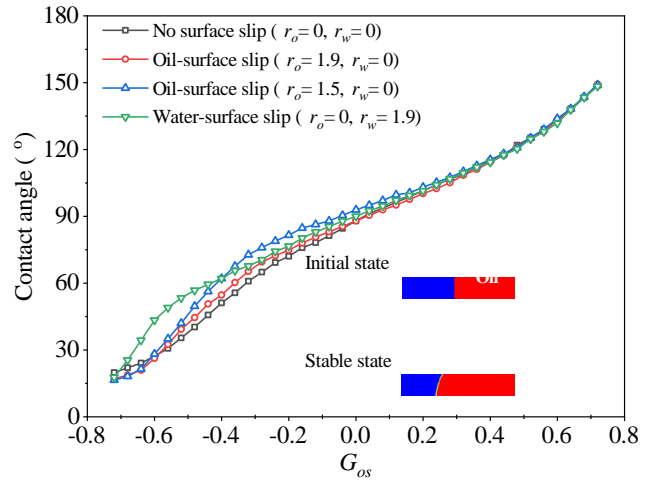


Fig. 1. Oil contact angle versus oil-solid interaction parameter and boundary conditions.

interfacial region can be modified to obtain the interfacial slip (Wang et al., 2019a; Zhan et al., 2020b), and the modified viscosity is called apparent viscosity. First, the phase-field equation $\rho^N = (\rho_\sigma - \rho_{\sigma'}) / (\rho_\sigma + \rho_{\sigma'})$ is used to track the oil-water interface region, and $\rho_\sigma = \sum_{\alpha} f_{\sigma, \alpha}$ is the density of σ component. Then, the relaxation time τ in the interfacial region, which is related to the viscosity in the lattice, is modified in the interface region to obtain the interface slip. As τ decreases, the interfacial slip velocity increases.

The surface forces acting on the fluid molecules in the near-wall region and those in the bulk region are drastically different. As a result, the fluid viscosity in the near-wall phase is different from that in the bulk phase (Mattia and Calabrò, 2012; Wang et al., 2019b; Zhang et al., 2020a). The near-wall relaxation time τ_{wall} and bulk relaxation time τ_{bulk} can be used to obtain the heterogeneous viscosity.

3. Model verification

The IFT, wettability, fluid-surface slip and fluid-fluid interfacial slip obtained by the proposed model should be verified to ensure its accuracy. The verification of IFT and fluid-fluid interfacial slip can be found in our previous works (Wang et al., 2022), and the lattice IFT γ equals 0.123. In this section, the oil-water contact angle and fluid-surface slip in LBM simulations are verified.

In Shan-Chen LBM, the different contact angles can be obtained by varying fluid-surface interaction parameter $G_{\sigma s}$ in Eq. (4). In this work, the water-surface interaction force G_{ws} is equal to minus oil-surface interaction force G_{os} ($G_{ws} = -G_{os}$), and the relation between oil-water contact angle is $\theta_w = 180^\circ - \theta_o$. In the simulation, a square oil phase is first placed on the surface which is saturated with water phase. Under the effect of oil/water-surface interaction force and oil-water IFT, the square oil phase gradually transforms to imperfect-circular droplets. Through the bottom length and height of the imperfect-circular droplet, the oil droplet contact angle can be calculated, as shown in Fig. 1. With various boundary conditions, different contact angles can be calculated. As the oil-surface interaction force G_{os} increases, the oil contact angle

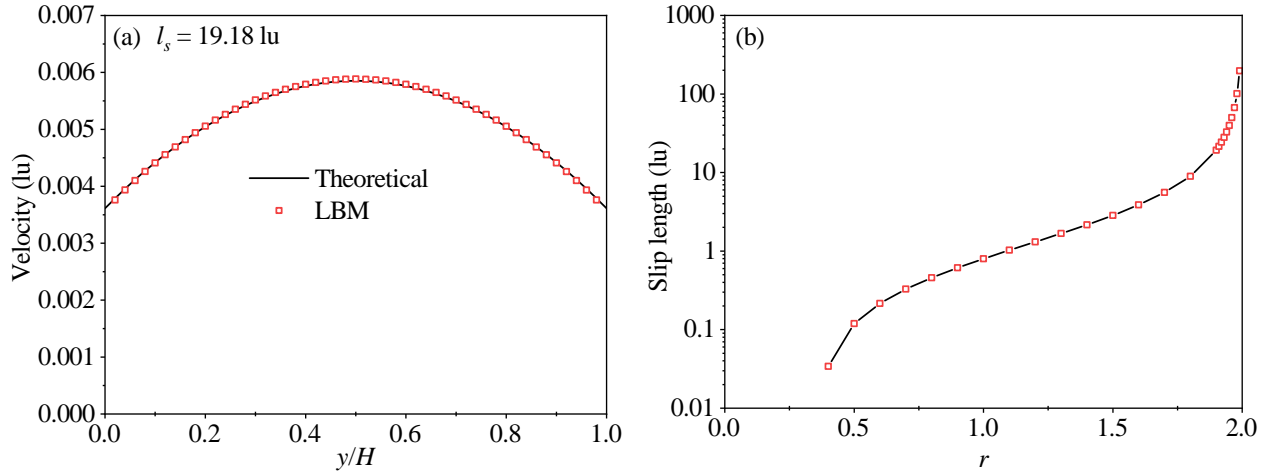


Fig. 2. Velocity fitting, and the relation between slip length and combined parameter. (a) Velocity, (b) slip length.

Table 1. Parameters used in LBM simulations.

Parameters	No slip	Oil slip	Oil slip
θ_w ($^\circ$)	30	30	30
θ_o ($^\circ$)	150	150	150
r_w	0	0	0
r_o	0	1.5	1.9
l_{sw} (nm)	0	0	0
l_{so} (nm)	0	0.56	3.84
G_{ws}	-0.719	-0.720	-0.717
G_{os}	0.719	0.720	0.717

increases.

In addition, the model in this work can also achieve different oil-water boundary slip lengths by changing the boundary conditions. The slip boundary conditions have a non-negligible impact on the oil-water contact angle (Wang et al., 2022). Therefore, for different slip boundary conditions, it is necessary to establish the corresponding relation between contact angle and oil/water-surface interaction force. In the proposed model, different slip lengths can be realized by varying slip boundary combination parameters. However, the relationship between the combined parameter r and the boundary slip length is not clear in the previous study (Wang et al., 2022). In this section, this relationship by theoretical fitting method is established. First, the fluid flow in the pore is simulated with pore width $H = 50$ lu, the combined parameter $r = 1.9$, and the external body force acceleration $F_{\sigma,b,x} = 0.000002$. The left and right boundary conditions of the pore are periodic, and the upper and lower boundary is half-way bounce back and diffusive Maxwell's reflection. The velocity profile is shown in Fig. 2(a). Then, the slip length l_s in the theoretical equation $u(y) = (y(H-y)/2\nu\rho_\sigma + l_s H/2\nu\rho_\sigma)F_{\sigma,b,x}$ is adjusted until the calculated velocity profile is fitted to the simulated velocity profile, where is theoretical velocity and is lattice kinematic viscosity. With perfect fitting, the corresponding slip

length with the combined parameter $r = 1.9$ is 19.18 lu. As shown in Fig. 2(b), with increasing slip boundary combination parameters r_o and r_w , the oil-surface and water-surface slip length increases.

4. Results and discussion

In this section, the effect of pore size, fluid-surface slip, water film, oil-water interfacial slip, water bridge and pore structures on the imbibition behaviors in nanopores is investigated. Then, the spontaneous imbibition behaviors in quartz nanoporous media are discussed.

4.1 Effect of pore size and fluid-surface slip

The pore sizes are equal to 3.6 nm, 6.2 nm, 9.0 nm, 11.4 nm and 17.8 nm, respectively. From previous studies, the slip velocity of water in hydrophilic quartz pores is 0, while there is a non-zero slip velocity of the oil phase in quartz pores (Zhan et al., 2020b; Wang et al., 2022). Therefore, this study only focuses on the effect of oil phase slip length on imbibition behaviors. The slip boundary conditions include non-slip boundary ($l_w = 0$ lu, $l_o = 0$ lu, and lu is lattice unit), oil phase slip boundary ($l_w = 0$ lu, $l_o = 2.8$ lu), and oil phase slip boundary ($l_w = 0$ lu, $l_o = 19.2$ lu), with the length scale $L_o = 0.2$ nm and the physical slip length $l_{o-phy} = l_o L_o$. The contact angle of the water and oil phase are $\theta_w = 30^\circ$ and $\theta_o = 150^\circ$, respectively. Unless otherwise specified, the corresponding parameters used in the following simulations are given in Table. 1.

The pore model used in the LBM simulation is shown in Fig. 3. The model length is 120 nm (the lattice length is 600 lu), and the length of the pore is 70 nm (the lattice length is 350 lu). With different widths, the pores with different pore sizes can be obtained. Periodic boundary conditions are applied to the upper, lower, left and right boundaries. At the initial state, the pores are saturated with oil, while the outer area is saturated with water.

During imbibition simulation, the oil-water distributions with lattice time at 5,000 lu and 20,000 lu are shown in Figs. 4

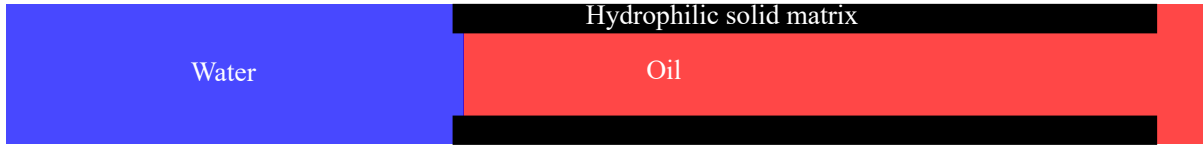


Fig. 3. The pore model used in LBM simulation.

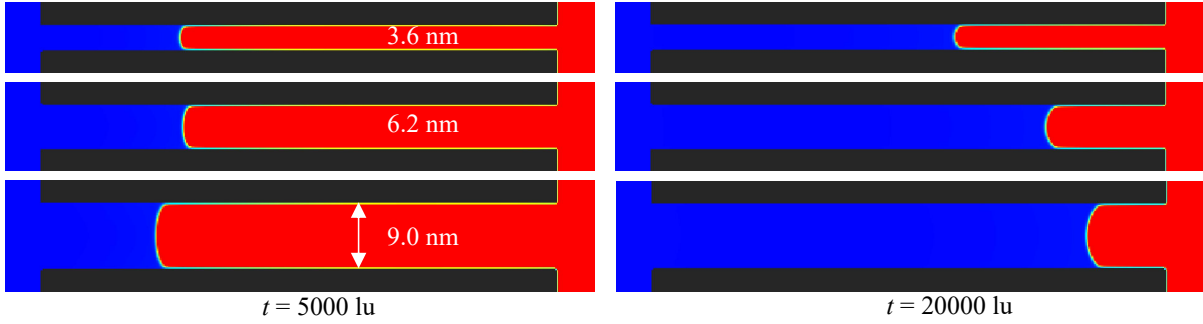


Fig. 4. oil-water distributions during imbibition process.

and 5 show the dependence of imbibition length on pore size and time under different boundary conditions. In the initial stage, the smaller the pore size, the larger the imbibition length is observed. With the increase of time, the imbibition velocity in the pore with a smaller pore size decreases gradually. Then, in the late stage of the imbibition process, the smaller the pore size, the smaller the imbibition length. Under the condition of no slip and oil slip boundary, the effect of pore size on imbibition length can all be reversed with time. The reversed law can be explained by the dynamics contact angle (resulting in different capillary pressure), hydrodynamic resistance and inertia force. When the inertia force is not considered, the capillary pressure is used entirely to drive oil and water flow. The capillary pressure equals the sum of pressure differences acting on the oil and water phases, i.e. $P_c = \Delta P_w + \Delta P_o$, where ΔP_w and ΔP_o are the pressure differences acting on the water and oil phases, which are related to the hydrodynamic resistance. The hydrodynamic resistance is defined as the ratio of pressure difference to average velocity to characterize the flow capacity of water and oil phases in nanopores. The water (R_w) and oil (R_o) hydrodynamic resistances are given by $R_w = \Delta P_w / \bar{u}_w$ and $R_o = \Delta P_o / \bar{u}_o$, where \bar{u}_w and \bar{u}_o are the average velocity of water and oil phase during the imbibition process, and $\bar{u}_w = \bar{u}_o = Q_w / A = Q_o / A$. Q_w and Q_o are the volume flux of water and oil phases, A is the cross-sectional area of the pore. During the imbibition process, the volume of water imbibed into the pore is equal to that of oil displaced $Q_w = Q_o$, and the detailed calculation can be found in our previous study (Wang et al., 2021b). Then, the total hydrodynamic resistance without considering the inertia force can be expressed by $R_t = \Delta P_w / \bar{u}_w + \Delta P_o / \bar{u}_o = (\Delta P_w + \Delta P_o) / u_t = P_c / u_t$.

For a slit pore, the capillary pressure is determined by the Young-Laplace equation $P_c = 2\gamma \cos \theta / H$, where γ is water-oil interfacial tension, θ is the dynamics contact angle. The imbibition velocity without considering the inertia force can be calculated by the capillary pressure and

total hydrodynamic resistance, $u_t = P_c / R_t = 2\gamma \cos \theta / HR_t$. In LBM simulations, the dynamics contact angle can be calculated from the meniscus shape of the imbibition front, as shown in Fig. 6. According to the dynamics contact angle, the lattice oil-water interfacial tension and pore size, the capillary pressure can be calculated. From our previous study (Wang et al., 2021a), the ideal total hydrodynamic resistance is given by $R_t = L_w (H^2 / 12\mu_{w\text{eff}} + l_w H / 2\mu_{nw})^{-1} + L_o (H^2 / 12\mu_{o\text{eff}} + l_o H / 2\mu_{no})^{-1}$, where L_w is the imbibition length shown in Fig. 5, $L_o = L_t - L_w$, L_t is pore length, $\mu_{w\text{eff}}$ and $\mu_{o\text{eff}}$ are the water and oil effective viscosity determined by the viscosity of near-wall and bulk phases. The total hydrodynamic resistance is shown in Fig. 7. Then, based on dynamics contact angle and hydrodynamic resistance, the imbibition velocity without considering inertia force versus pore size and time is shown in Fig. 8. It shows that the imbibition velocity decreases with the decreasing pore size because the hydrodynamic resistance of pore with a small size is much larger than that with a large size. Therefore, when the inertial force is not taken into account, the smaller the pore size is, the smaller the imbibition length should be. It is consistent with the conclusion in our previous theoretical studies (Wang et al., 2021a) without considering the inertial force, while inconsistent with the reversed law versus time from LBM simulations. Then, the simulation results by considering inertial forces are analyzed in the following paragraph.

When the inertia force is considered, the pressure equilibrium relation can be expressed by $P_c = \Delta P_w + \Delta P_o + P_i$, then, the imbibition velocity is $u_t = 2\gamma_{ow} \cos \theta / HR_t - P_i / R_t$. In the initial stage of imbibition, the inertia force cannot be ignored because the larger the pore size, the greater the inertia force (Weibing et al., 2022). According to the velocity formula, in the early stage of imbibition, the small imbibition length arises from the large inertia force and small hydrodynamic resistance in the pore with a large size. With the increase of imbibition

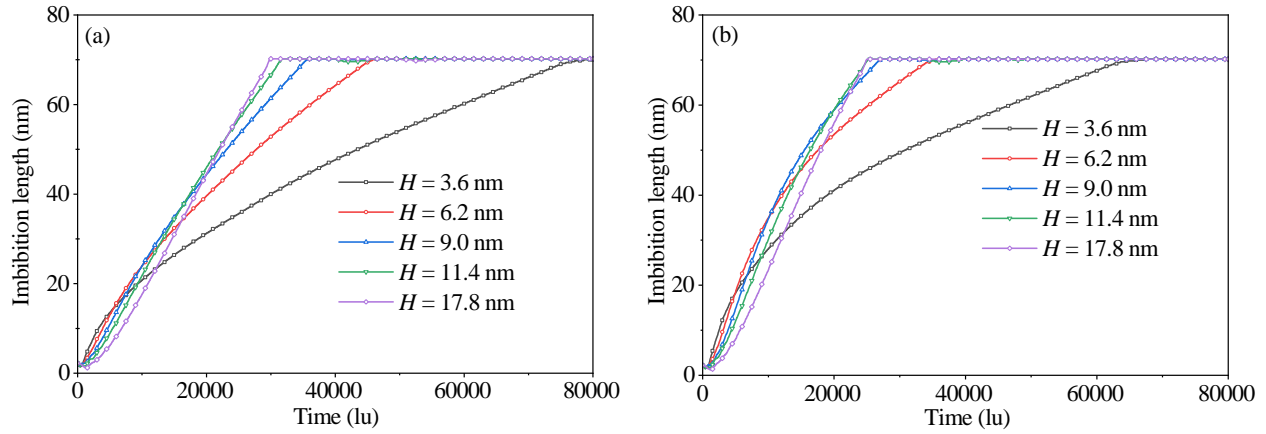


Fig. 5. Imbibition length versus time and pore diameter. (a) No slip, (b) oil slip ($r_o = 1.9$).

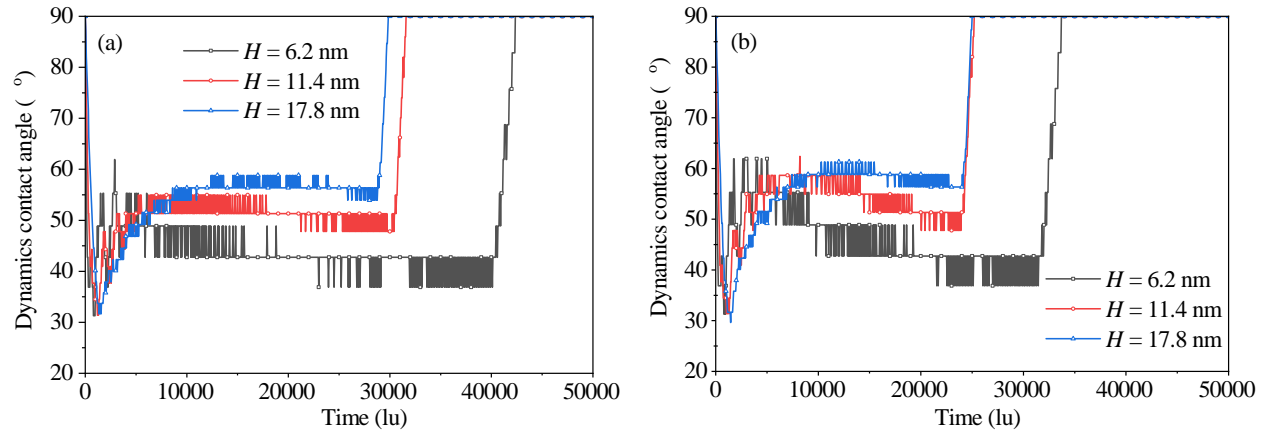


Fig. 6. Dynamics contact angle versus time and pore diameter. (a) No slip, (b) oil slip ($r_o = 1.9$).

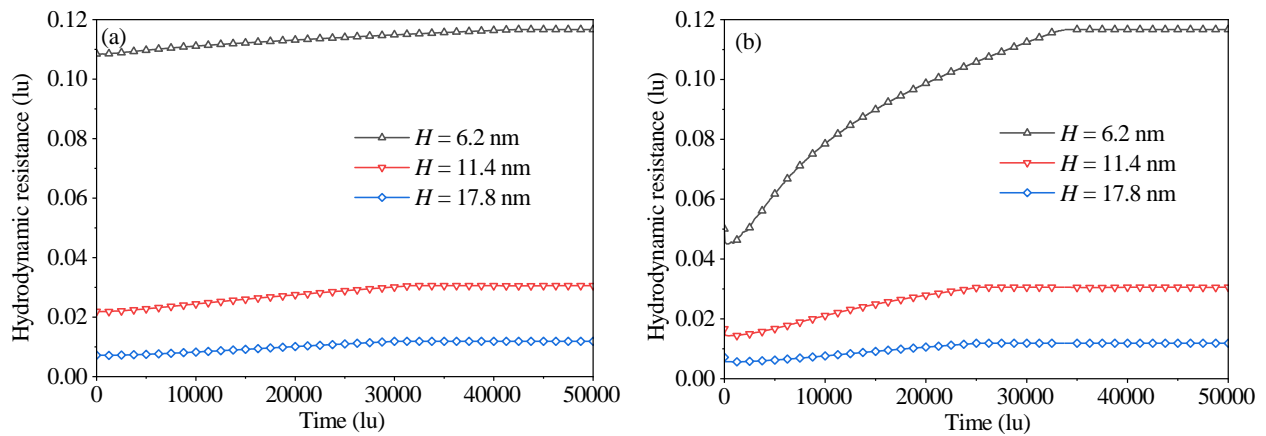


Fig. 7. Hydrodynamic resistance versus time and pore diameter. (a) No slip, (b) oil slip ($r_o = 1.9$).

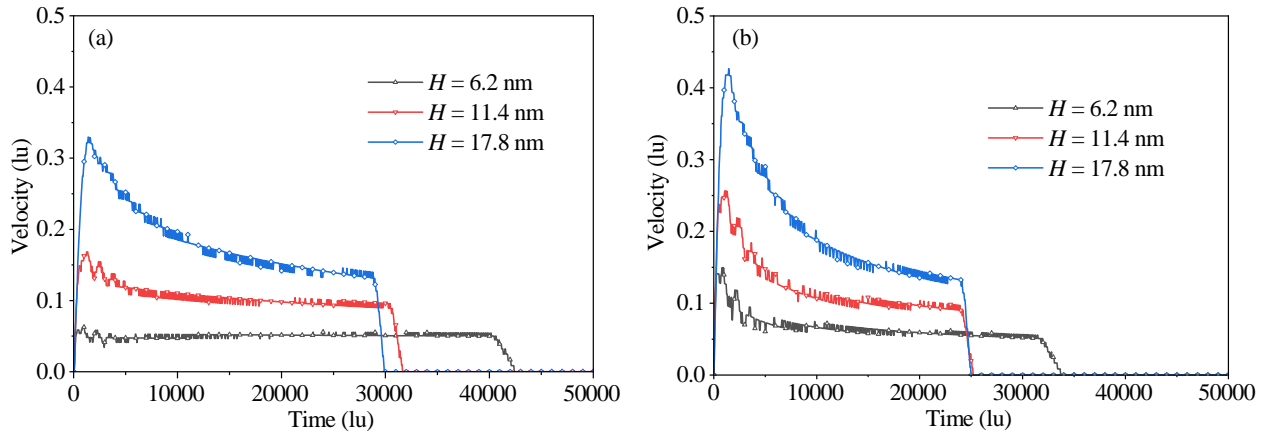


Fig. 8. Velocity $v_t = P_c/R_t$ versus time and pore size. (a) No slip, (b) oil slip ($r_o = 1.9$).

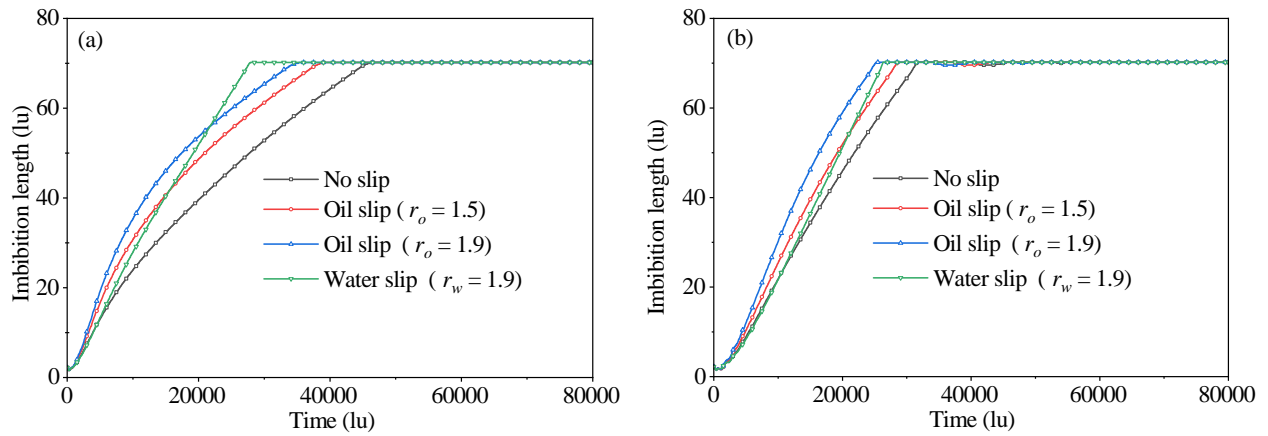


Fig. 9. Imbibition length versus time and boundary condition. (a) $H = 6.2$ nm, (b) $H = 11.4$ nm.

time, the inertia force gradually decreases and approaches zero (Weibing et al., 2022). Then, the capillary pressure and hydrodynamic resistance dominate the imbibition process, as shown in Figs. 5-8, and the imbibition velocity decreases with the increase of pore size.

The variation of imbibition length with time and boundary conditions is shown in Fig. 9. With an increasing slip length, the imbibition length increases due to the decreasing hydrodynamic resistance of oil-water flow in the pores.

4.2 Effect of water film and oil-water interfacial slip

When the initial water saturation in the porous media is low, the water phase exists on the solid surface of the hydrophilic pores as a water film based on previous MD simulations (Li et al., 2018; Wang et al., 2022). It can be seen that there is a slip velocity at the oil-water interfacial region (Xu et al., 2022). Fig. 10 shows the oil-water distributions during the imbibition process considering water film and different oil-water interfacial slips. The pore width H is 11.4 nm, and the thickness of the water film is 2 nm. The oil-water interfacial relaxation time τ_{ow} is used to obtain the desired oil-water interfacial slip. With a decrease of τ_{ow} , the oil-water

interfacial slip length increases. As shown in Fig. 11, when the water film is considered, the effective pore size of water phase imbibition decreases, however, the imbibition length increases which is inconsistent with that in section 4.1. There are two potential reasons: One is that due to the oil-water interfacial slip, the hydrodynamic resistance decreases; The other one is that the water film can be regarded as a solid surface, which is completely hydrophilic, and then the capillary force increases. Therefore, the presence of water film is conducive to imbibition. With an increasing oil-water interfacial slip length, the imbibition length increases because of the decrease in hydrodynamic resistance.

4.3 Effect of water bridge

The attractive interactions caused by surface forces directly affect water film stability. At a certain local water saturation (critical water film thickness), the wetting film will form a water bridge (Guan et al., 2016; Li et al., 2017). In this part, the influences of the water bridge on imbibition behaviors are studied. With and without water bridge imbibition, the oil-water distributions are shown in Fig. 12. With water bridge, there are three capillary pressures formed by imbibition meniscus, two of which are the driving force and one is the

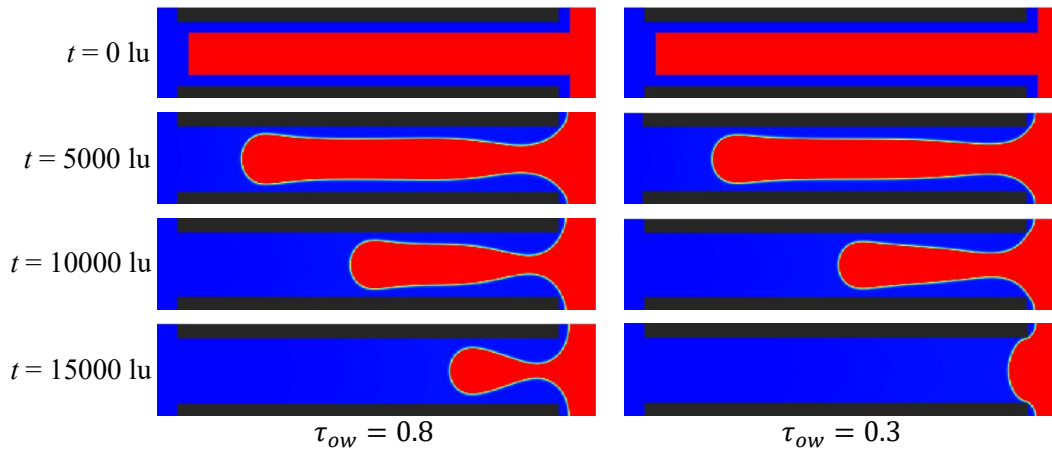


Fig. 10. Oil-water distributions.

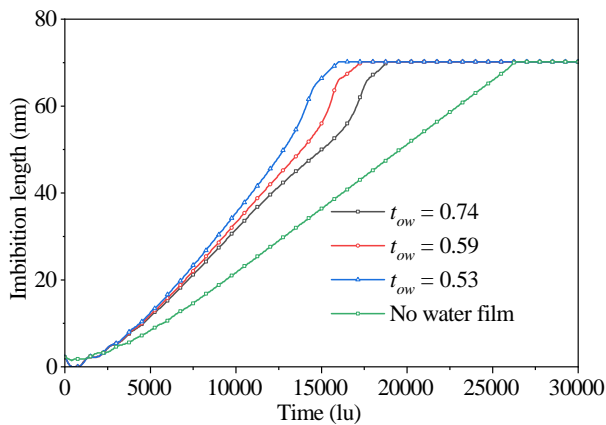


Fig. 11. Imbibition length versus oil-water interfacial slip length.

resistance. According to the dynamics contact angle as depicted in Fig. 13(a), the dynamics contact angle with the water bridge is small resulting in great capillary pressure, and the total capillary pressure is $P_1 + P_3$. However, the net driving force ($P_1 + P_3 - P_2$) is small, and the existence of a water bridge (no slip velocity in the water phase) increases the hydrodynamic resistance of oil-water flow. Therefore, the imbibition length is greatly reduced, as shown in Fig. 13(b). When the water bridge reaches the pore outlet, the capillary force on the left and right ends of the oil phase in the pore reaches balance, and this part of the oil is trapped inside the pores and cannot be exchanged by spontaneous imbibition.

4.4 Effect of pore structures

Oil production by spontaneous imbibition from pores can occur in both co- and counter-current modes when the matrix is partially covered by water (Meng et al., 2019). The imbibition mentioned above is a co-current process, and the counter-current process is discussed in this section. The simulation model is that the two pores are connected, and the small pore width is fixed at 8 nm. Then the ratio of large pore width to small pore width (H_{ratio}) is 1.2, 1.5 and 2 by changing the lar-

Table 2. Parameters fitted from MD simulations.

Parameters	Value
Near-wall oil viscosity (mPa·s)	0.5
Bulk oil viscosity (mPa·s)	0.9
Oil slip combination parameter	1.858
Near-wall water viscosity (mPa·s)	5
Bulk water viscosity (mPa·s)	1
Water slip combination parameter	0
Liquid-liquid slip parameter	0.59

ge pore width. Fig. 14 shows the oil-water distribution when the pore width ratio is 1.2 and 2. Fig. 15 shows the imbibition length in the pore with a small width versus width ratio and time. Due to the great capillary back pressure $P_{1,2}$ and high hydrodynamic resistance, the imbibition length decreases with a decrease in the pore size ratio.

4.5 Imbibition behaviors in quartz porous media

To study the imbibition behaviors in quartz porous media, which is the main mineral composition, the physical parameters in the proposed model can be adjusted by MD simulations. For oil and water flow in quartz nanopores, we recently used MD simulation to investigate a laminar-type oil-water two-phase flow in quartz nanopores (Zhan et al., 2020b), in which oil and water single-phase as well as two-phase velocity profiles can be obtained. Then, by the velocity fitting (the detailed fitting can be found in our previous studies (Wang et al., 2022)), the physical parameters of oil/water near-wall viscosity, boundary slip, IFT, and liquid-liquid slip can be obtained, as shown in Table 2.

The circular two-dimensional porous media is constructed. The porous media is initially saturated with oil and then surrounded by water. During imbibition simulation, the water phase flows into the porous media by spontaneous imbibition and the oil phase is displaced. Fig. 16 shows the time depen-

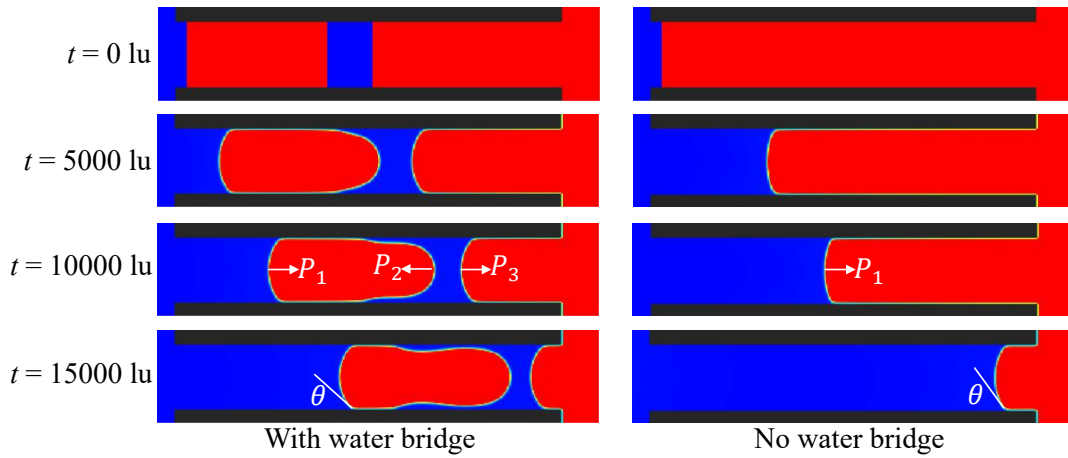


Fig. 12. Oil-water distributions.

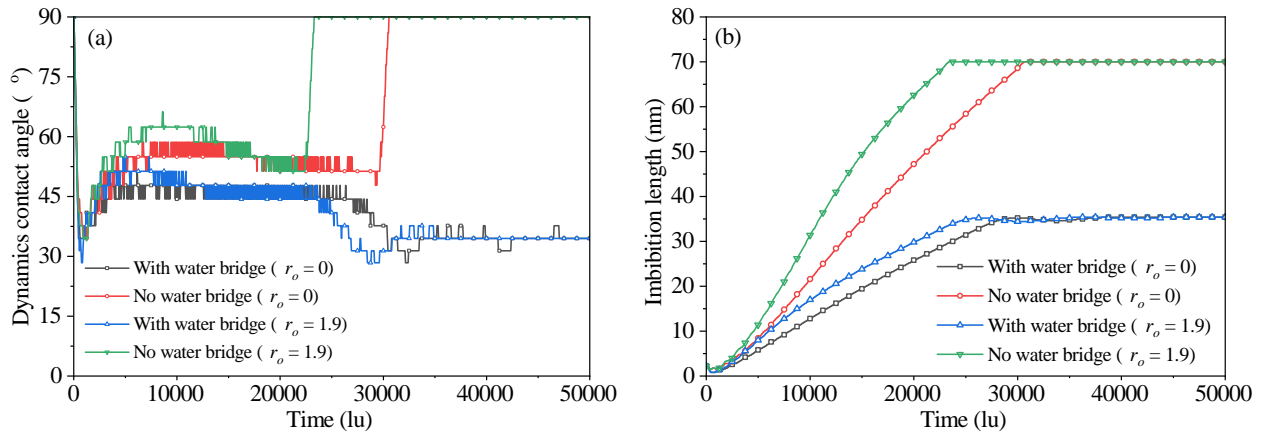


Fig. 13. Dynamics contact angle and imbibition length versus water bridge and time. (a) Dynamics contact angle, (b) imbibition length.

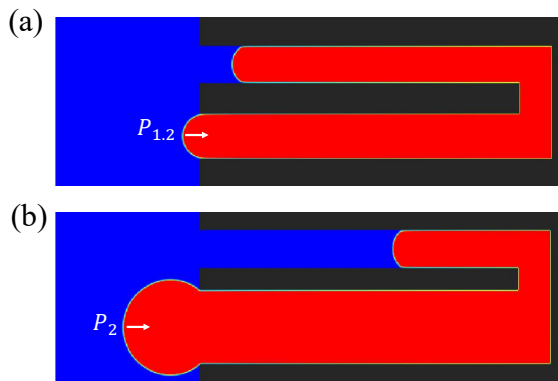


Fig. 14. Oil-water distribution. (a) $H_{ratio} = 1.2$, (b) $H_{ratio} = 2$.

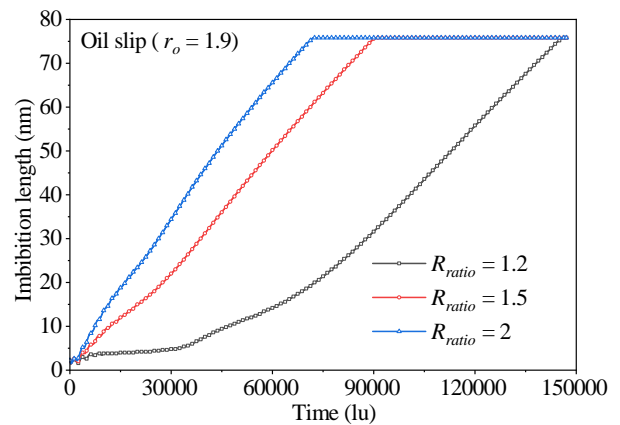


Fig. 15. Imbibition length versus width pore width ratio and time.

dence of oil-water distributions at different water saturation. The imbibition mass versus time and water saturation is shown in Figs. 17(a) and 17(b). As the water saturation increases from 0 to 0.1, the imbibition mass increases. It is because the small amount of water forms a film on the solid wall, and the oil-water interfacial slip and a completely hydrophilic wall (lead-

ing to increased capillary pressure) make an increasing imbibition mass. As water saturation continues to increase, imbibition mass decreases gradually because the existence of the water bridge impedes the water imbibition.

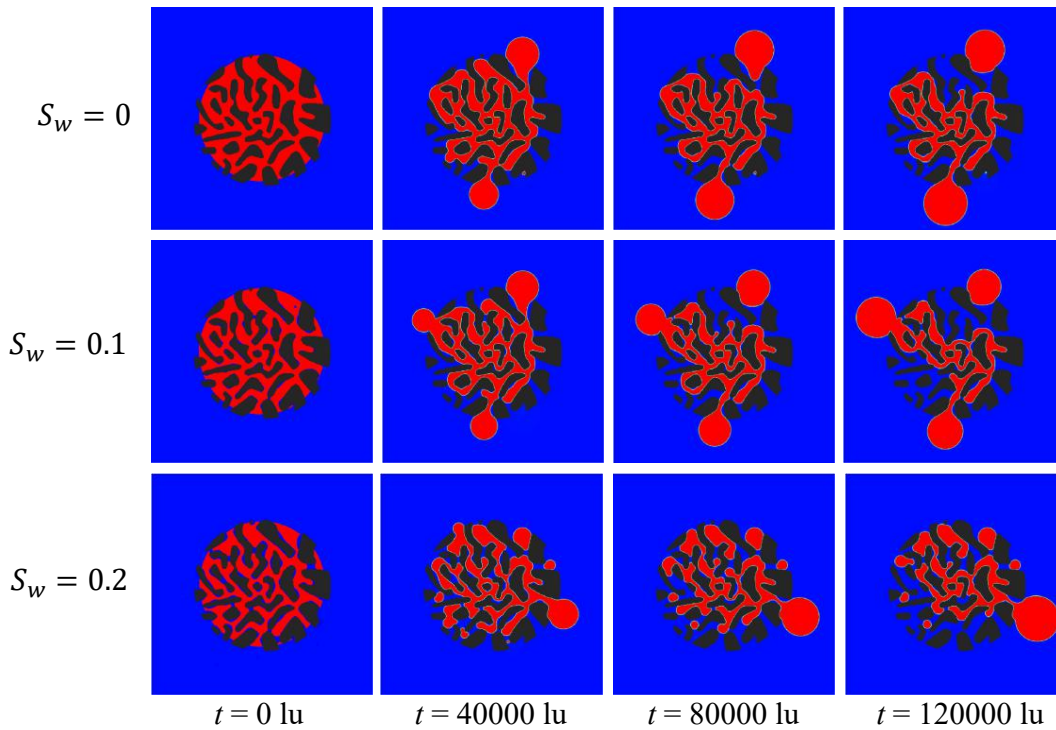


Fig. 16. Oil-water distributions with different water saturation.

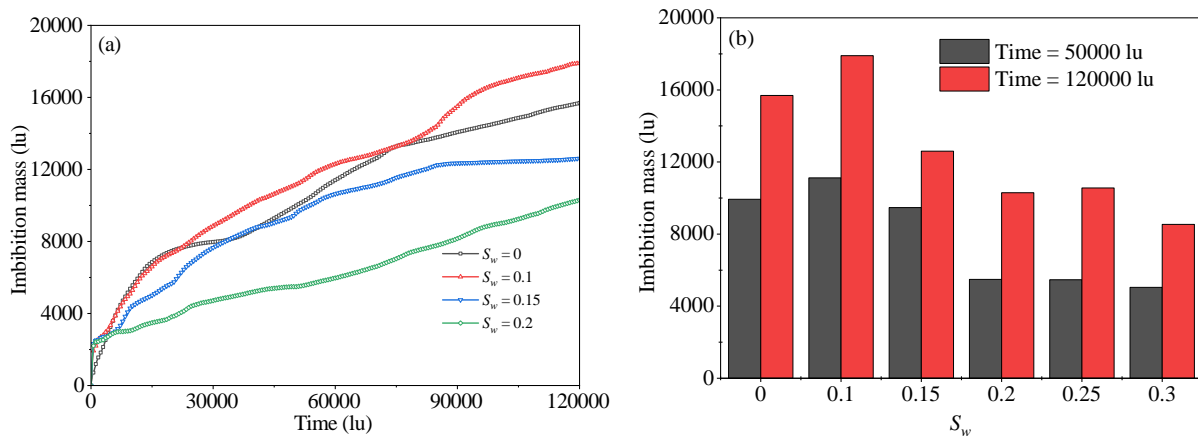


Fig. 17. Imbibition mass versus time and water saturation. (a) Time, (b) water saturation.

5. Conclusions

In this work, a nanoscale multi-relaxation-time multicomponent and multiphase LBM is applied to investigate the water flow into nanoscale space by spontaneous imbibition. The effects of pore size, fluid-surface slip, water film, oil-water interfacial slip, water bridge and pore structures on the imbibition behaviors are investigated. Then, the spontaneous imbibition behaviors in quartz nanoporous media are simulated based on the pore scale microsimulation parameters obtained from the molecular simulation velocity results, and the effect of water saturations in porous media is discussed.

The results show that the imbibition length decreases first

and then increases with the increase of pore size due to the influence of hydrodynamic resistance and inertia force of oil-water flow in nanopores. With an increasing oil-surface slip length, the imbibition length increases due to the decreasing hydrodynamic resistance. The presence of water film and oil-water interfacial slip is conducive to imbibition, because of the increase in capillary force and the decrease in imbibition resistance due to the solid-like water film and interfacial slip, respectively. The water bridge can increase the capillary resistance, therefore, the imbibition length is greatly reduced. In the connected pores with different pore sizes, due to the great capillary back pressure and high hydrodynamic resistance with a small pore size ratio, the imbibition length decreases. With

the water saturation increases from 0 to 0.1, the imbibition mass in quartz nanoporous media increases. It is because the small amount of water forms a film on the solid wall, and the oil-water interfacial slip and a completely hydrophilic wall (leading to increased capillary pressure) make an increasing imbibition mass. As water saturation continues to increase, the imbibition mass decreases gradually because the existence of water bridges impedes the water imbibition.

Acknowledgements

This study was supported by the National Natural Science Foundation of China (Nos. 42172159, 51974348), a Discovery Grant from Natural Sciences and Engineering Research Council of Canada (NSERC RGPIN-2017-05080) and China Postdoctoral Science Foundation (No. 2023M733872).

Conflict of interest

The authors declare no competing interest.

Open Access This article is distributed under the terms and conditions of the Creative Commons Attribution (CC BY-NC-ND) license, which permits unrestricted use, distribution, and reproduction in any medium, provided the original work is properly cited.

References

- Abd, A. S., Elhafyan, E., Siddiqui, A. R., et al. A review of the phenomenon of counter-current spontaneous imbibition: Analysis and data interpretation. *Journal of Petroleum Science and Engineering*, 2019, 180: 456-470.
- Akbarabadi, M., Saraji, S., Piri, M., et al. Nano-scale experimental investigation of in-situ wettability and spontaneous imbibition in ultra-tight reservoir rocks. *Advances in Water Resources*, 2017, 107: 160-179.
- Al-Ameri, A., Gamadi, T., Ispas, I. Evaluation of the near fracture face formation damage caused by the spontaneously imbibed fracturing fluid in unconventional gas reservoirs. *Journal of Petroleum Science and Engineering*, 2018, 171: 23-36.
- Cai, J., Chen, Y., Liu, Y., et al. Capillary imbibition and flow of wetting liquid in irregular capillaries: A 100-year review. *Advances in Colloid and Interface Science*, 2022, 304: 102654.
- Cai, J., Jin, T., Kou, J., et al. Lucas-washburn equation-based modeling of capillary-driven flow in porous systems. *Langmuir*, 2021, 37(5): 1623-1636.
- Chen, L., He, A., Zhao, J., et al. Pore-scale modeling of complex transport phenomena in porous media. *Progress in Energy and Combustion Science*, 2022, 88: 100968.
- Chen, M., Yan, M., Kang, Y., et al. Stress sensitivity of multiscale pore structure of shale gas reservoir under fracturing fluid imbibition. *Capillarity*, 2023, 8(1): 11-22.
- Chen, C., Zhuang, L., Li, X., et al. A many-body dissipative particle dynamics study of forced water-oil displacement in capillary. *Langmuir*, 2012, 28(2): 1330-1336.
- Deng, H., Sheng, G., Zhao, H., et al. Integrated optimization of fracture parameters for subdivision cutting fractured horizontal wells in shale oil reservoirs. *Journal of Petroleum Science and Engineering*, 2022, 212: 110205.
- Feng, D., Li, X., Wang, X., et al. Anomalous capillary rise under nanoconfinement: A view of molecular kinetic theory. *Langmuir*, 2018, 34(26): 7714-7725.
- Guan, Q., Dong, D., Wang, S., et al. Preliminary study on shale gas microreservoir characteristics of the lower silurian longmaxi formation in the southern sichuan basin, China. *Journal of Natural Gas Science and Engineering*, 2016, 31: 382-395.
- Hodder, K. J., Nychka, J. A. Silane treatment of 3D-printed sandstone models for improved spontaneous imbibition of water. *Transport in Porous Media*, 2019, 129(2): 583-598.
- Kannam, S. K., Daivis, P. J., Todd, B. Modeling slip and flow enhancement of water in carbon nanotubes. *MRS Bulletin*, 2017, 42(4): 283-288.
- Lallemant, P., Luo, L. S. Theory of the lattice boltzmann method: Dispersion, dissipation, isotropy, galilean invariance, and stability. *Physical Review E*, 2000, 61(6): 6546.
- Li, J., Chen, Z., Wu, K., et al. Effect of water saturation on gas slippage in circular and angular pores. *AIChE Journal*, 2018, 64(9): 3529-3541.
- Li, J., Li, X., Wang, X., et al. Water distribution characteristic and effect on methane adsorption capacity in shale clay. *International Journal of Coal Geology*, 2016, 159: 135-154.
- Li, J., Li, X., Wu, K., et al. Thickness and stability of water film confined inside nanoslits and nanocapillaries of shale and clay. *International Journal of Coal Geology*, 2017, 179: 253-268.
- Li, C., Singh, H., Cai, J. Spontaneous imbibition in shale: A review of recent advances. *Capillarity*, 2019, 2(2): 17-32.
- Li, G., Su, Y., Wang, W., et al. Mathematical model and application of spontaneous and forced imbibition in shale porous media-considered forced pressure and osmosis. *Energy & Fuels*, 2022, 36(11): 5723-5736.
- Liu, Y., Berg, S., Ju, Y., et al. Systematic investigation of corner flow impact in forced imbibition. *Water Resources Research*, 2022, 58(10): e2022WR032402.
- Liu, J., Sheng, J. J., Wang, X., et al. Experimental study of wettability alteration and spontaneous imbibition in chinese shale oil reservoirs using anionic and nonionic surfactants. *Journal of Petroleum Science and Engineering*, 2019, 175: 624-633.
- Lu, H., Xu, Y., Duan, C., et al. Experimental study on capillary imbibition of shale oil in nanochannels. *Energy & Fuels*, 2022, 36(10): 5267-5275.
- Mattia, D., Calabrò, F. Explaining high flow rate of water in carbon nanotubes via solid-liquid molecular interactions. *Microfluidics and Nanofluidics*, 2012, 13(1): 125-130.
- Mehmani, A., Kelly, S., Torres-Verdín, C., et al. Capillary trapping following imbibition in porous media: Microfluidic quantification of the impact of pore-scale surface roughness. *Water Resources Research*, 2019, 55(11): 9905-9925.
- Meng, Q., Cai, Z., Cai, J., et al. Oil recovery by spontaneous imbibition from partially water-covered matrix blocks with different boundary conditions. *Journal of Petroleum Science and Engineering*, 2019, 172: 454-464.

- Patil, P. D., Rohilla, N., Katiyar, A., et al. Surfactant based model for tight oil reservoirs through wettability alteration: Novel surfactant formulations and their efficacy to induce spontaneous imbibition. Paper SPE 190397 Presented at SPE EOR Conference at Oil and Gas West Asia, Muscat, Oman, 26-28 March, 2018.
- Ruiz-Morales, Y., Alvarez-Ramírez, F. Mesoscale dissipative particle dynamics to investigate oil asphaltenes and sodium naphthenates at the oil-water interface. *Energy & Fuels*, 2021, 35(11): 9294-9311.
- Sang, Q., Zhao, X., Liu, H., et al. Analysis of imbibition of n-alkanes in kerogen slits by molecular dynamics simulation for characterization of shale oil rocks. *Petroleum Science*, 2022, 19(3): 1236-1249.
- Saputra, I. W. R., Park, K. H., Zhang, F., et al. Surfactant-assisted spontaneous imbibition to improve oil recovery on the eagle ford and wolfcamp shale oil reservoir: Laboratory to field analysis. *Energy & Fuels*, 2019, 33(8): 6904-6920.
- Saraji, S., Piri, M. The representative sample size in shale oil rocks and nano-scale characterization of transport properties. *International Journal of Coal Geology*, 2015, 146: 42-54.
- Secchi, E., Marbach, S., Nigues, A., et al. Massive radius-dependent flow slippage in carbon nanotubes. *Nature*, 2016, 537(7619): 210-213.
- Shao, W., Yang, J., Wang, H., et al. Recent research progress on imbibition system of nanoparticle-surfactant dispersions. *Capillarity*, 2023, 8(2): 34-44.
- Sheng, J. What type of surfactants should be used to enhance spontaneous imbibition in shale and tight reservoirs? *Journal of Petroleum Science and Engineering*, 2017, 159: 635-643.
- Siddhamshetty, P., Wu, K., Kwon, J. S.-I. Modeling and control of proppant distribution of multistage hydraulic fracturing in horizontal shale wells. *Industrial & Engineering Chemistry Research*, 2019, 58(8): 3159-3169.
- Siddiqui, M. A. Q., Chen, X., Iglauer, S., et al. A multiscale study on shale wettability: Spontaneous imbibition versus contact angle. *Water Resources Research*, 2019, 55(6): 5012-5032.
- Singh, H. A critical review of water uptake by shales. *Journal of Natural Gas Science and Engineering*, 2016, 34: 751-766.
- Tsao, C. W., Huang, Q., You, C., et al. The effect of channel aspect ratio on air entrapment during imbibition in soil-on-a-chip micromodels with 2D and 2.5D pore structures. *Lab on a Chip*, 2021, 21(2): 385-396.
- Tu, J., Sheng, J. J. Effect of pressure on imbibition in shale oil reservoirs with wettability considered. *Energy & Fuels*, 2020, 34(4): 4260-4272.
- Wang, S., Javadpour, F., Feng, Q. Molecular dynamics simulations of oil transport through inorganic nanopores in shale. *Fuel*, 2016, 171: 74-86.
- Wang, X., Sheng, J. J. Spontaneous imbibition analysis in shale reservoirs based on pore network modeling. *Journal of Petroleum Science and Engineering*, 2018, 169: 663-672.
- Wang, X., Sheng, J. J. Dynamic pore-scale network modeling of spontaneous water imbibition in shale and tight reservoirs. *Energies*, 2020, 13(18): 4709.
- Wang, H., Su, Y., Wang, W., et al. Relative permeability model of oil-water flow in nanoporous media considering multi-mechanisms. *Journal of Petroleum Science and Engineering*, 2019a, 183: 106361.
- Wang, H., Su, Y., Wang, W. Investigations on water imbibing into oil-saturated nanoporous media: Coupling molecular interactions, the dynamic contact angle, and the entrance effect. *Industrial Engineering Chemistry Research*, 2021a, 60(4): 1872-1883.
- Wang, H., Su, Y., Zhao, Z., et al. Apparent permeability model for shale oil transport through elliptic nanopores considering wall-oil interaction. *Journal of Petroleum Science and Engineering*, 2019b, 176: 104152.
- Wang, W., Wang, H., Su, Y., et al. Simulation of liquid flow transport in nanoscale porous media using lattice boltzmann method. *Journal of the Taiwan Institute of Chemical Engineers*, 2021b, 121: 128-138.
- Wang, H., Wang, W., Su, Y., et al. Lattice boltzmann model for oil/water two-phase flow in nanoporous media considering heterogeneous viscosity, liquid/solid, and liquid/liquid slip. *SPE Journal*, 2022, 27(6): 3508-3524.
- Wang, W., Xie, Q., Wang, H., et al. Pseudopotential-based multiple-relaxation-time lattice boltzmann model for multicomponent and multiphase slip flow. *Advanced in Geo-Energy Research*, 2023, 9(2): 106-116.
- Weibing, T., Kelu, W., Zhangxing, C., et al. Mathematical model of dynamic imbibition in nanoporous reservoirs. *Petroleum Exploration and Development*, 2022, 49(1): 170-178.
- Wijaya, N., Sheng, J. Effects of imbibition during well shut-in on ultimate shale oil recovery: A numerical study. *SPE Reservoir Evaluation & Engineering*, 2021, 24(4): 859-873.
- Wiklund, H. S., Uesaka, T. Microfluidics of imbibition in random porous media. *Physical Review E*, 2013, 87(2): 023006.
- Wu, K., Chen, Z., Li, J., et al. Wettability effect on nanoconfined water flow. *Proceedings of the National Academy of Sciences*, 2017, 114(13): 3358-3363.
- Wu, K., Chen, Z., Li, J., et al. Nanoconfinement effect on n-alkane flow. *Journal of Physical Chemistry C*, 2019, 123(26): 16456-16461.
- Xu, G., Han, Y., Jiang, Y., et al. Reducing residual oil saturation: Underlying mechanism of imbibition in oil recovery enhancement of tight reservoir. *SPE Journal*, 2021, 26(4): 2340-2351.
- Xu, J., Zhan, S., Wang, W., et al. Molecular dynamics simulations of two-phase flow of n-alkanes with water in quartz nanopores. *Chemical Engineering Journal*, 2022, 430: 132800.
- Yang, S., Dehghanpour, H., Binazadeh, M., et al. A molecular dynamics explanation for fast imbibition of oil in organic tight rocks. *Fuel*, 2017, 190: 409-419.
- Yuan, Y., Wang, Y., Rahman, S. S. Reconstruction of porous structure and simulation of non-continuum flow in shale

- matrix. *Journal of Natural Gas Science and Engineering*, 2017, 46: 387-397.
- Zeng, F., Zhang, Q., Guo, J., et al. Capillary imbibition of confined water in nanopores. *Capillarity*, 2020, 3(1): 8-15.
- Zhan, S., Su, Y., Jin, Z., et al. Effect of water film on oil flow in quartz nanopores from molecular perspectives. *Fuel*, 2020a, 262: 116560.
- Zhan, S., Su, Y., Jin, Z., et al. Study of liquid-liquid two-phase flow in hydrophilic nanochannels by molecular simulations and theoretical modeling. *Chemical Engineering Journal*, 2020b, 395: 125053.
- Zhang, T., Javadpour, F., Li, X., et al. Mesoscopic method to study water flow in nanochannels with different wettability. *Physical Review E*, 2020a, 102(1): 013306.
- Zhang, T., Javadpour, F., Yin, Y., et al. Upscaling water flow in composite nanoporous shale matrix using lattice boltzmann method. *Water Resources Research*, 2020b, 56(4): e2019WR026007.
- Zhang, T., Li, X., Shi, J., et al. An apparent liquid permeability model of dual-wettability nanoporous media: A case study of shale. *Chemical Engineering Science*, 2018, 187: 280-291.
- Zhang, Q., Su, Y., Wang, W., et al. Apparent permeability for liquid transport in nanopores of shale reservoirs: Coupling flow enhancement and near wall flow. *International Journal of Heat and Mass Transfer*, 2017, 115: 224-234.
- Zhao, J., Qin, F., Fischer, R., et al. Spontaneous imbibition in a square tube with corner films: Theoretical model and numerical simulation. *Water Resources Research*, 2021, 57(2): e2020WR029190.
- Zhao, J., Qin, F., Kang, Q., et al. A dynamic pore network model for imbibition simulation considering corner film flow. *Water Resources Research*, 2022, 58(7): e2022WR032332.
- Zheng, J., Ju, Y., Wang, M. Pore-scale modeling of spontaneous imbibition behavior in a complex shale porous structure by pseudopotential lattice boltzmann method. *Journal of Geophysical Research: Solid Earth*, 2018, 123(11): 9586-9600.
- Zhou, Y., Guan, W., Zhao, C., et al. Spontaneous imbibition behavior in porous media with various hydraulic fracture propagations: A pore-scale perspective. *Advances in Geo-Energy Research*, 2023, 9(3): 185-197.
- Zhou, S., Yan, G., Xue, H., et al. 2D and 3D nanopore characterization of gas shale in longmaxi formation based on fib-sem. *Marine and Petroleum Geology*, 2016, 73: 174-180.
- Zhu, G., Kou, J., Yao, B., et al. Thermodynamically consistent modelling of two-phase flows with moving contact line and soluble surfactants. *Journal of Fluid Mechanics*, 2019, 879: 327-359.